BIOSYSTEMS ENGINEERING 99 (2008) 496–507

Available at www.sciencedirect.com

ScienceDirect

journal homepage: www.elsevier.com/locate/issn/15375110

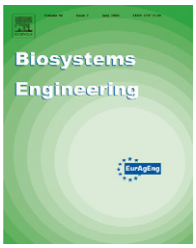

Research Paper: PM—Power and Machinery

Centrifugal spreading of fertiliser: Deducing three-dimensional velocities from horizontal outlet angles using computer vision

S. Villette[a,*], E. Piron[b], F. Cointault[a], B. Chopinet[a]

[a]ENESAD, DSI-LGAP, BP 87999, 21079 Dijon Cedex, France
[b]Cemagref, Les Palaquins, 03150 Montoldre, France

ARTICLE INFO

Article history:
Received 28 May 2007
Accepted 3 December 2007
Available online 14 January 2008

The quality of the deposit pattern produced by centrifugal spreaders is known to depend on many parameters, making its prediction using models based on fertiliser properties and disc settings difficult. An alternative approach consists of measuring the initial conditions of the ballistic flight of the fertiliser particles as they leave the disc, thus avoiding the use of on-spinner dynamic models. Measurement methods need to be developed to determine the outlet velocity vector of the particles in three dimensions. Using kinematic analysis of the mechanical system, this paper establishes that the three-dimensional velocity components of the particles are functions of the horizontal outlet angle, the disc configuration and the rotational speed. The theoretical relationship between the vertical and the horizontal outlet angles was also derived from this analysis. A digital imaging system was developed to measure the horizontal outlet angle and thus estimate the velocity components. In order to avoid any bias regarding the angle determination, special attention was paid to image acquisition and measurement corrections. Experiments have been carried out to assess the technique.

© 2007 IAgrE. Published by Elsevier Ltd. All rights reserved.

1. Introduction

In Europe, the application of granular fertilisers onto agricultural fields is mainly performed using centrifugal spreaders. Despite the mechanical simplicity of these farm implements, the quality of the spreading depends on many parameters, including particle properties and machine characteristics. Consequently, because of difficulties in adjusting the machines, major differences in the quality of the spread pattern deposition can be observed in the field. Indeed, numerous studies have reported a lack of uniformity in fertiliser spreading when the transverse distribution is assessed in the field (Ziani & Rousselet, 1990a; Tissot *et al.*, 1999; Leterme, 2000; Roussel, 2006). This adversely affects not only the crops (Ziani & Rousselet, 1990b; Tissot *et al.*, 1999; Leterme, 2000) but also the environment (Tissot *et al.*, 2002), especially in the case of nitrogen-based fertilisers.

Economic and environmental considerations call for improvements in the quality of fertiliser spreading. Moreover, in the context of precision farming, site-specific fertiliser management implies the development of rate- and uniformity-controlled spreaders, using feedback control systems. As a result, there is a need to better understand and model the process of centrifugal spreading.

The spreading process consists of two main stages, namely the motion of the fertiliser particles on the spreader (i.e. from

*Corresponding author.
E-mail address: s.villette@enesad.fr (S. Villette).
1537-5110/$ - see front matter © 2007 IAgrE. Published by Elsevier Ltd. All rights reserved.
doi:10.1016/j.biosystemseng.2007.12.001

Nomenclature

A	intersection point between the disc axle and the ejection plane
A_p	particle frontal area, m^2
$\boldsymbol{a}_b$	acceleration vector of the particle during the ballistic flight, $m\,s^{-2}$
A_i	image of A on the CCD plane
C	origin of the camera frame
C_D	drag coefficient
d	diameter of the particle, m
d_c	diameter of the corresponding sphere, m
d_e	diameter of the equivalent sphere, m
E	point where a particle leaves the vane
E_i	image of E on the CCD plane
f	focal length of the lens, m
f_{conv}	metre per pixel conversion factor, m $pixel^{-1}$
$\boldsymbol{g}$	acceleration vector due to gravity, $m\,s^{-2}$
g	magnitude of the acceleration due to gravity, $m\,s^{-2}$
$\mathbf{i}_C$	vector of the camera frame (C, $\mathbf{i}_C$, $\boldsymbol{j}_C$, $\boldsymbol{k}_C$), lying on a horizontal plane
$\mathbf{i}_{ETim}$	vector lying along the considered trajectory image on the CCD
$\boldsymbol{j}_C$	vector of the camera frame (C, $\mathbf{i}_C$, $\boldsymbol{j}_C$, $\boldsymbol{k}_C$), lying on a horizontal plane
$\boldsymbol{j}_{ETim}$	vector perpendicular to the considered trajectory image on the CCD
K	coefficient of the dynamic model
K_1	coefficient of the dynamic model when $\mu = 1$
K_2	coefficient of the dynamic model when $\mu = 0$
K_a	aerodynamic coefficient m^{-1}
$\boldsymbol{k}$	vertical vector
$\boldsymbol{k}_C$	vertical vector of the camera frame (C, $\mathbf{i}_C$, $\boldsymbol{j}_C$, $\boldsymbol{k}_C$)
L_f	theoretical length of the ballistic flight, m
l_{vane}	length of the vane, m
m	particle mass, kg
O	point lying on the rotational axle of the disc
O_V	projection of O on the vane axis
P	principal point (intersection point between the image plane and the optical axis)
r	radial location of the particle with respect to O, m
r_p	pitch radius of the vane, m
r_{vane}	radius of the vane, m
T	trajectory
T_{Hor}	orthogonal projection of the trajectory on a horizontal plane
T_{im}	image of the trajectory on the CCD
u_i	first coordinate in the image, pixel
u_{i0}	first coordinate of the principal point, pixel
$\boldsymbol{u}_R$	vector of the moving frame (O, $\boldsymbol{u}_R$, $\boldsymbol{u}_T$, $\boldsymbol{k}$), lying on a horizontal plane
$\boldsymbol{u}_T$	vector of the moving frame (O, $\boldsymbol{u}_R$, $\boldsymbol{u}_T$, $\boldsymbol{k}$), lying on a horizontal plane
v	magnitude of the velocity vector, $m\,s^{-1}$
$\boldsymbol{v}$	velocity vector of the particle, $m\,s^{-1}$
$\boldsymbol{v}_b$	velocity vector of the particle during the ballistic flight, $m\,s^{-1}$
v_b	magnitude of the velocity during the ballistic flight, $m\,s^{-1}$
$\boldsymbol{v}_H$	horizontal component of the outlet velocity vector, $m\,s^{-1}$
v_H	magnitude of the horizontal component of the outlet velocity, $m\,s^{-1}$
v_i	second coordinate in the image, pixel
v_{i0}	second coordinate of the principal point, pixel
$\boldsymbol{v}_R$	horizontal radial component of the outlet velocity vector, $m\,s^{-1}$
v_R	magnitude of the horizontal radial component of the outlet velocity, $m\,s^{-1}$
$\boldsymbol{v}_T$	horizontal tangential component of the outlet velocity vector, $m\,s^{-1}$
v_T	magnitude of the horizontal tangential component of the outlet velocity, $m\,s^{-1}$
x_c	first coordinate in the camera frame, m
x_V	abscissa of the particle on the vane (with respect to O_V), m
$\dot{x}_V$	velocity of the particle along the vane, $m\,s^{-1}$
$\dot{x}_{Vout}$	velocity of the particle along the vane at the outer extremity of the vane, $m\,s^{-1}$
y_c	second coordinate in the camera frame, m
$y_{ETim}(P)$	ordinate of the principal point P in (E_i, $\mathbf{i}_{ETi}$, $\boldsymbol{j}_{ETi}$), pixel
z_c	third coordinate in the camera frame, m
α_x	angle between the horizontal projection of the vane and the radial location of the particle depending on x_V, rad
α_{lv}	pitch angle of the vane, rad
δ	coefficient of the model
δ_1	coefficient of the dynamic model when $\mu = 1$
δ_2	coefficient of the dynamic model when $\mu = 0$
ρ_T	radius parameter of the angle-radius description of a line, deg.
ρ_{air}	air density, $kg\,m^{-3}$
ρ_{part}	density of the fertiliser particle, $kg\,m^{-3}$
$\dot{\theta}$	magnitude of the rotational speed of the disc, $rad\,s^{-1}$
θ_{out}	horizontal outlet angle of the particle with respect to $\boldsymbol{v}_T$, deg.
θ_{out_im}	apparent outlet angle directly measured in the image, deg.
θ_{out_sim}	horizontal outlet angle simulated using a tightened rope, deg.
θ_{out_max}	maximum value of the horizontal outlet angle of the particle, deg.
θ_{out_min}	minimum value of the horizontal outlet angle of the particle, deg.
θ_T	angle parameter of the angle-radius description of a line, deg.
ε_θ	angular difference between θ_{out} and θ_{out_im}, deg.
μ	friction coefficient of the particle along the vane and the disc

Δl_f	difference concerning the theoretical length of flight, m	$\Delta\Omega_{out}$	difference concerning the vertical outlet angle, deg.
Δp	width of a square pixel, m	Ω	angle between the vane and the horizontal plane, deg.
Δp_x	width of a pixel, m	Ω_{out}	vertical outlet angle of the particle, deg.
Δp_y	height of a pixel, m	Ω_{out_sim}	vertical angle of a simulated trajectory, deg.

the hopper to the outer extremity of the vane) and the ballistic flight of the particles. Thus, to predict the spreading pattern, the initial velocity vectors of flight are required as input data by ballistic models. They can be provided either by modelling the motion on the spinning disc or by measuring these data in the vicinity of the disc.

In terms of modelling approaches, early studies addressed the motion of fertiliser particles for flat spinning discs equipped with simple radial vanes (Patterson & Reece, 1962; Inns & Reece, 1962). This was extended by Cunningham (1963), who studied the case of a flat disc with pitched vanes and also investigated the case of a concave disc with radial vanes. Cunningham and Chao (1967) further extended this to include the case of curved vanes. Several decades later, Hofstee (1995) provided the differential equations of the motion for various disc configurations especially cone-shaped discs equipped with pitched vanes. Olieslagers (1997) also studied these cases. Both authors established a non-linear differential equation which had to be solved numerically.

More recently, Villette *et al.* (2005) established a new form for the motion equation leading to an analytical solution. These studies demonstrated that the motion of a single particle on the vane depends on the disc configuration parameters and on the interaction between the particle and the vane, especially the friction coefficient. Thus, the use of these models to predict the outlet velocity of the particles required the measurement of fertiliser characteristics. Moreover, these dynamic studies are usually based on hypotheses that can have a significant impact, such as ignoring interactions between fertiliser particles. An alternative approach takes into account particle interactions using the discrete element method (Tijskens *et al.*, 2005; Van Liedekerke *et al.*, 2005). Quantitative simulations using this method would necessitate physical fertiliser characteristics which are currently unknown and difficult to measure.

Thus, although dynamic models are of particular interest in studying the qualitative effects of the influential parameters to design or optimise spreaders, they require calibration for each fertiliser to provide quantitative results. Hence, in practice, the accuracy of quantitative simulations is hindered by the lack of knowledge concerning the physical behaviour of the fertiliser on the vane.

In order to obtain the velocity of the fertiliser particles when they leave the vane, an alternative approach is to develop measurement methods and sensors in the vicinity of the disc. Various devices have been designed to measure exit velocity. Hofstee (1994) developed a technique based on the ultrasonic Doppler frequency shift using one transmitter and three receivers arranged in a three-dimensional configuration. The measurement of the cell opening was 20 mm × 20 mm. Grift and Hofstee (1997) developed an optical sensor using two photosensitive arrays, placed perpendicularly with respect to the radius of the disc. The radial component of the outlet velocity was derived from the time difference corresponding to a particle passing each sensor array. The orifice of the measurement unit was 30 mm. Using this device as a spread pattern determination sensor, Grift and Hofstee (2002) showed that because of the sensor mounting configuration the true velocity was higher than that measured. This implies that only the radial component of the velocity was measured. The authors suggested that a solution could be to turn the sensor to seek the direction and the magnitude of the maximum velocity. Cointault and Vangeyte (2005) presented various stroboscopic imaging systems to measure the outlet velocity of fertiliser granules. With these techniques, the velocity was deduced from the displacement of the particles in the image between two successive flashes or lighting strobes. In contrast to the stroboscopic approach, Villette *et al.* (2006) developed an automatic image processing technique to derive the outlet angle and the outlet velocity from motion-blurred images on which particle trajectories appear as straight streaks owing to continuous lighting during the exposure of a CCD camera. All these imaging systems are available for flat discs, assuming that the particle trajectories are parallel to the image plane. Nevertheless, in the case of concave discs, these methods do not provide the vertical components of the velocity. Furthermore, when the trajectories are not parallel to the image plane, distance measurements or angle measurements deduced from images are biased. As a result, the available techniques are either limited to a narrow investigated space, are difficult to apply or assume that the particles move in a horizontal plane. Consequently, no technique is currently available to estimate the outlet velocity in three dimensions or to estimate the vertical outlet angle of the particles.

Regarding the motion of fertiliser particles on a spinning disc, most of the mechanical studies, in the literature, focus on the dynamic analysis of the motion in order to obtain the magnitude of the velocity of the particles when they leave the disc, whereas kinematic relationships between the velocity components have aroused little interest. Thus, for concave discs, various methods have been used to determine the vertical component of the outlet velocity when the global magnitude is estimated. Olieslagers *et al.* (1996) and Colin (1997) considered the vertical angle of the outlet velocity vector as the cone angle of the disc. However, Olieslagers (1997) defined the vertical outlet angle by the arc-tangent of the horizontal to vertical ratio of the outlet velocity components and suggested a difference from the vertical vane or disc angle. Nevertheless, the expression of this angle was not established. Likewise, Dintwa *et al.* (2004) distinguished the vertical outlet angle from the vertical vane angle but did not suggest any analytical expression. To compute ballistic flight

simulations, Reumers *et al.* (2003b) measured the horizontal outlet angle and the vertical outlet angle separately to determine, respectively, the horizontal and the vertical components of the outlet velocity. Thus, no relationship is currently available in the literature to link the horizontal and the vertical outlet angles of the particles leaving a spinning disc.

The aim of this paper is to demonstrate that in the case of a concave disc (equipped with radial or pitched vanes), the three-dimensional components of the outlet velocity can be deduced from the measurement of the horizontal outlet angle and that there is a simple relationship between the vertical and the horizontal outlet angles. Regarding the measurement of the horizontal outlet angle, the present paper extends the imaging system presented by Villette *et al.* (2006) to the general case of concave discs which are more common, and demonstrates that the three-dimensional velocity can be extracted from a single motion-blurred image.

2. Theoretical considerations

2.1. Three-dimensional components of the outlet velocity

The three-dimensional components of the outlet velocity are obtained using only the kinematic study of the motion of a fertiliser particle along the vane of a spinning disc. To describe the kinematic behaviour of the particle during its centrifugal acceleration on the disc, (O, $\boldsymbol{u}_R$, $\boldsymbol{u}_T$, $\boldsymbol{k}$) is defined as a right-handed Cartesian coordinate system having its origin O on the rotational axle of the disc with $\boldsymbol{u}_R$ in the direction of the particle projection on the horizontal plane passing through O and with $\boldsymbol{k}$ pointing upward (Fig. 1).

Considering a concave disc, equipped with backward pitched vanes, assuming a constant rotational speed $\dot{\theta}$ and deriving the location vector of a particle on the disc, Villette *et al.* (2005) demonstrated that the expression of the velocity of the particle is as follows:

$$\upsilon = (\dot{x}_V \cos\Omega\cos\alpha_x)\boldsymbol{u}_R + (r\dot{\theta} - \dot{x}_V\cos\Omega\sin\alpha_x)\boldsymbol{u}_T + (\dot{x}_V\sin\Omega)\boldsymbol{k} \quad (1)$$

where $\dot{x}_V$ is the velocity of the particle along the vane, r is the radial location of the particle, Ω is the angle between the vane and the horizontal plane and α_x is the horizontal angle between the vane and the radius of the particle location (Fig. 1).

When the particle leaves the vane, r equals the radius of the vane r_{vane} and α_x equals the pitch angle of the vane α_{lv} which is defined by

$$\alpha_{lv} = \arcsin\left(\frac{r_p}{r_{vane}}\right)$$

Consequently, at the extremity of the vane, the radial $\boldsymbol{v}_R$, the tangential $\boldsymbol{v}_T$ and the vertical $\boldsymbol{v}_k$ components of the outlet velocity are:

$$\mathbf{v}_R = (\dot{x}_{Vout}\cos\Omega\cos\alpha_{lv})\boldsymbol{u}_R \quad (2)$$

$$\mathbf{v}_T = \left(r_{vane}\dot{\theta} - \dot{x}_{Vout}\cos\Omega\sin\alpha_{lv}\right)\boldsymbol{u}_T \quad (3)$$

$$\upsilon_k = (\dot{x}_{Vout}\sin\Omega)\boldsymbol{k} \quad (4)$$

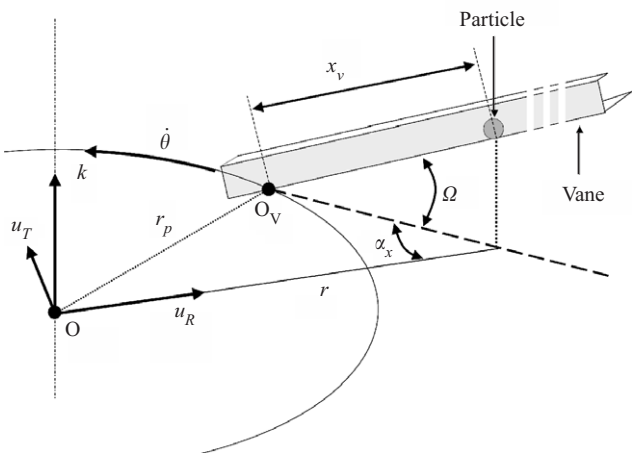

Fig. 1 – Three-dimensional view of the vane and of the coordinate system for a concave disc equipped with pitched vanes: O, point lying on the rotational axle of the disc; O_V, projection of O on the vane axis (lying in the same horizontal plane as O); (O, u_R, u_T, k), moving frame with u_R in the direction of the particle projection in the horizontal plane passing through O; r_p, pitch radius of the vane; r, radial location of the particle; x_V, abscissa of the particle on the vane; α_x, angle between the horizontal projection of the vane and the radial location of the particle; Ω, angle between the vane and the horizontal plane; $\dot{\theta}$, rotational speed of the disc.

where $\dot{x}_{Vout}$ is the velocity of the particle along the vane axis at the outer extremity of the vane.

From Eqs. (2) to (4), we observe that the components of the velocity vector depend solely on one unknown parameter which is $\dot{x}_{Vout}$. Three of the four other parameters are directly linked to the disc configuration (Ω, α_{lv}, r_{vane}), whereas the rotational speed $\dot{\theta}$ is easily measured or deduced from the power-take-off speed.

To circumvent the difficulties associated with estimating $\dot{x}_{Vout}$ and to avoid the dependence of any dynamic analysis of the motion of the particles on the vane, this unknown parameter has to be eliminated from the outlet velocity components. This is made possible by introducing a new piece of information concerning the behaviour of the fertiliser particles when they leave the vane, which is the horizontal outlet angle.

The horizontal outlet angle θ_{out} of the particle is defined as the angle of the horizontal component of the velocity $\boldsymbol{v}_H$ with respect to the tangential component $\boldsymbol{v}_T$ (Fig. 2). This yields:

$$\upsilon_T = \frac{\upsilon_R}{\tan\theta_{out}} \quad (5)$$

Combining Eqs. (2) and (3) provides:

$$\upsilon_T = r_{vane}\dot{\theta} - \upsilon_R\tan\alpha_{lv} \quad (6)$$

Substituting Eq. (5) into (6), the radial component of the velocity is obtained as follows:

$$\upsilon_R = \frac{r_{vane}\dot{\theta}\tan\theta_{out}}{1+\tan\theta_{out}\tan\alpha_{lv}} \quad (7)$$

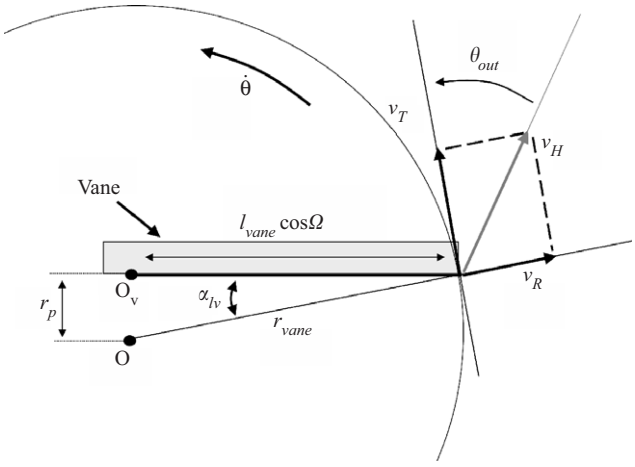

Fig. 2 – Top view of the spinning disc and components of the outlet velocity of the particle: v_H, horizontal component of the outlet velocity; v_R, horizontal radial component of the outlet velocity; v_T, horizontal tangential component of the outlet velocity; O, point lying on the rotational axle of the disc; O_V, projection of O on the vane axis; l_{vane}, length of the vane; r_p, pitch radius of the vane; r_{vane}, radius of the vane; α_{lv}, pitched angle of the vane; $\dot{\theta}$, rotational speed of the disc; Ω, angle between the vane and the horizontal plane.

Then, the tangential and the horizontal components are simply deduced:

$$v_T = \frac{v_R}{\tan\theta_{out}} = \frac{r_{vane}\dot{\theta}}{1+\tan\theta_{out}\tan\alpha_{lv}} \tag{8}$$

$$v_H = \frac{v_R}{\sin\theta_{out}} = \frac{r_{vane}\dot{\theta}}{\cos\theta_{out}+\sin\theta_{out}\tan\alpha_{lv}} \tag{9}$$

Combining Eqs. (2), (4) and (7), the vertical component of the outlet velocity is obtained:

$$v_k = \frac{v_R}{\cos\alpha_{lv}}\tan\Omega = \frac{r_{vane}\dot{\theta}\tan\theta_{out}}{\cos\alpha_{lv}+\tan\theta_{out}\sin\alpha_{lv}}\tan\Omega \tag{10}$$

One way to express the magnitude of the absolute velocity is to consider the horizontal component and the vertical outlet angle:

$$v = \frac{v_H}{\cos\Omega_{out}} = \sqrt{1+\left(\frac{\sin\theta_{out}}{\cos\alpha_{lv}}\tan\Omega\right)^2} \times \frac{r_{vane}\dot{\theta}}{\cos\theta_{out}+\sin\theta_{out}\tan\alpha_{lv}} \tag{11}$$

Using this kinetic study of the particle motion on the spinning disc, the absolute velocity and the three-dimensional components of the velocity vector are expressed as functions of the horizontal outlet angle and some other known parameters (rotational speed and disc configuration). Consequently, the velocity components will be deduced from the measurement of the horizontal outlet angle. It is worth noting that using this approach to express the velocity components, no assumptions are made concerning the dynamic behaviour of the particle, especially concerning the friction coefficient.

This study was carried out using backward-pitched vanes. In the case of forward-pitched vanes, the distance r_p between the vane and the disc rotation axle has to be replaced by the negative value $-r_p$. Likewise, α_{lv} must be replaced by $-\alpha_{lv}$.

2.2. Vertical outlet angle

The kinematic analysis unequivocally answers questions concerning the vertical outlet angle. The angle Ω_{out} of a particle when it leaves the vane is deduced from Eqs. (9) and (10):

$$\Omega_{out} = \arctan\left(\frac{v_k}{v_H}\right) = \arctan\left(\frac{\sin\theta_{out}}{\cos\alpha_{lv}}\tan\Omega\right) \tag{12}$$

Thus, it appears that the vertical outlet angle Ω_{out} can be simply deduced from the disc configuration and the horizontal outlet angle θ_{out}, whose value depends on the behaviour of the fertiliser particles on the vane.

With a view to studying the consequences of this finding, the obtainable values for the horizontal outlet angle can be estimated using the theoretical expression deduced from the dynamic analysis established by Villette *et al.* (2005). In the case of a concave disc equipped with pitched straight vanes, and assuming that particles slide along the vane, the horizontal outlet angle is as follows:

$$\theta_{out} = \arctan\left(\frac{(l_{vane}-K)(\delta-\mu\cos\Omega)l_{vane}\cos^2\Omega}{r_{vane}^2-(l_{vane}-K)(\delta-\mu\cos\Omega)r_p\cos\Omega}\right) \tag{13}$$

where μ is the friction coefficient of the particles along the vane and the disc and K and δ are coefficients whose expressions are given in Appendix A.

In practice, it will be readily assumed that the friction coefficient is higher than 0 and lower than 1. This bounded domain includes fertiliser friction values widely reported in the literature (e.g. Hofstee & Huisman, 1990; Hofstee, 1992; Grift *et al.*, 2006). It follows that the value range for θ_{out} is included between θ_{out_min} and θ_{out_max} whose expressions are given in Appendix B.

Substituting θ_{out_min} or θ_{out_max} into Eq. (12) provides the limiting values of the vertical outlet angle. By way of an example, these values have been computed for the case of a concave disc equipped with pitched vanes which is available in the laboratory. The disc configuration and working parameters are: $\Omega = 10.7^\circ$, $r_p = -24$ mm, $r_{vane} = 391$ mm and $\dot{\theta} = 800$ rpm. In this case, the minimum and the maximum values of the horizontal angle are approximately 17° and 43°. Therefore, when deducing the vertical outlet angle of the particles from Eq. (12), the minimum value is 3.1° and the maximum value is 7.3°, that is to say from approximately 30% to 70% of the vertical angle of the vane. This illustrates that the vertical outlet angle of the particle is noticeably smaller than the vertical angle of the vane.

One particular case can be examined to underline the importance of the vertical outlet angle in predicting the ballistic flight and spread pattern deposition. Considering a spherical particle which is located at 700 mm above the floor when it leaves the vane and for which the diameter is 3 mm, the density is 1800 kg m^{-3} and the drag coefficient is 0.44. The length of its predicted ballistic flight would be 15.9 m if the vertical outlet angle equalled the vane angle ($\Omega = 10.7^\circ$)

of the previous example. However, the flight lengths would be 14.1 and 11.2 m, respectively, when the vertical outlet angle is assumed to be 7.3° and 3.1°. This involves differences from approximately 10% to 30% in terms of the theoretical flight length when the vertical outlet angle is used compared to the length obtained when the vane angle value is used.

Eq. (12) also demonstrates that the vertical outlet angle decreases with the friction coefficient since the horizontal outlet angle decreases when the friction coefficient μ increases (Eq. (13)). As a result, for one concave disc configuration, fertilisers with a high friction coefficient not only reach a lower outlet velocity because of their lower horizontal outlet angle θ_{out} but also have a lower vertical outlet angle Ω_{out}. In addition to the effect of their drag coefficient during ballistic flight, the combined effect of these considerations involves lower flight lengths for high-friction-coefficient fertilisers.

2.3. *Outlet angle measurement with the pinhole camera model*

Let us consider the measurement of the outlet angle of the particles using a CCD camera placed above the output flow in the vicinity of the spinning disc. The orientation of the camera is assumed to afford the view axis parallel to the disc axle. The camera consists of an image plane and a lens to provide the transformation between the object space and the image space. Let us define the camera coordinate system (C, $\mathbf{i}_C$, $\mathbf{j}_C$, $\mathbf{k}_C$) as a right-handed Cartesian system taking its origin at the lens focus and with $\mathbf{k}_C$ in the view axis direction.

Assuming a perfect acquisition system, the geometrical relationships between the coordinates ($x_C(M)$, $y_C(M)$, $z_C(M)$) of the point M in the scene, according to the camera system, and the coordinates ($u_i(M)$,$v_i(M)$) of its projection on the CCD plane, are deduced from the pinhole model (Fig. 3) as follows:

$$\begin{pmatrix} u_i(M) \\ v_i(M) \\ 1 \end{pmatrix} = \frac{1}{z_C(M)} \begin{bmatrix} f/\Delta p_x & 0 & u_{i0} & 0 \\ 0 & f/\Delta p_y & v_{i0} & 0 \\ 0 & 0 & 1 & 0 \end{bmatrix} \begin{pmatrix} x_C(M) \\ y_C(M) \\ z_C(M) \\ 1 \end{pmatrix} \quad (14)$$

where f is the focal length of the lens, Δp_x is the pixel width, Δp_y is the pixel height and (u_{i0}, v_{i0}) are the coordinates of the principal point P in the image (i.e. the intersection point of the view axis with the image plane).

In the image, the location of a pixel is defined with respect to the upper left-hand corner with u_i in the line direction and v_i in the column direction. Assuming that the pixels are square, we can note $\Delta p_x = \Delta p_y = \Delta p$ where Δp is the pixel width. In the case of a flat spinning disc, since the image plane is parallel to the motion plane, the outlet angle measured in the image θ_{out_im} is the outlet angle θ_{out} of the particle. On the other hand, in the case of a concave disc, the particle trajectories do not lie in the same plane during spreading and are not parallel to the image plane (Fig. 3). Consequently, there is a difference between the orientation of the trajectories in the image and the orientation that their horizontal components actually have. Thus, the apparent outlet angle directly measured in the image θ_{out_im} is not the real horizontal outlet angle θ_{out} of the particle. The angular

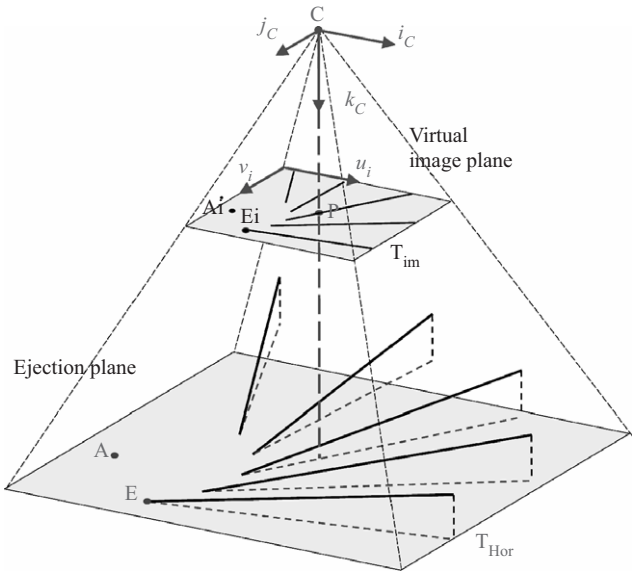

Fig. 3 – Three-dimensional simulation of tilted trajectories with orthogonal projection on the ejection plane and with pinhole camera projections in the virtual image plane: (C, i_C, j_C, k_C) camera frame; (u_i, v_i) location coordinates in the image; A, intersection point between the disc axle and the ejection plane; E, point where a particle leaves the vane; A_i, image of A in the CCD plane; E_i, image of E in the CCD plane; P, principal point; T_{Hor} orthogonal projection of the trajectory on the horizontal ejection plane, T_{im} image of the trajectory on the CCD plane.

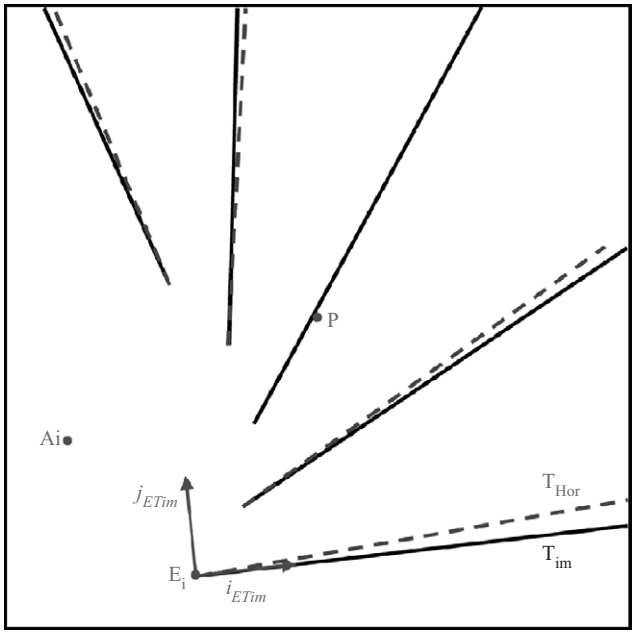

Fig. 4 – Pinhole camera projections of the trajectories (continuous lines) and of their horizontal components (dotted lines) corresponding to the situation represented in Fig. 3: A_i, image of A in the CCD plane, P, principal point; T_{im} image of the trajectory on the CCD plane, T_{Hor} image on the horizontal component of the trajectory, (E_i, i_{ETim}, j_{ETim}) trajectory image frame.

bias between the two directions is illustrated in Fig. 4 for five trajectories.

The expression of this angular bias ε_θ is established using a geometric decomposition of the image acquisition based on the pinhole camera model. The method consists in noting that the distance between the lens focus and the trajectory is unknown, except for the ejection point. This point belongs to the trajectory but it also corresponds to the extremity of the vane and its third coordinate $z_C(E)$ is perfectly known in the camera frame.

Considering a right-handed Cartesian coordinate system $(E_i, \mathbf{i}_{ETim}, \mathbf{j}_{ETim})$ with E_i the image of the ejection point and with $\mathbf{i}_{ETim}$ collinear to the trajectory (Fig. 4), the expression of the angular bias ε_θ is established as follows:

$$\varepsilon_\theta = \theta_{out} - \theta_{out\_im} = \arcsin\left(-y_{ETim}(P)\tan(\Omega_{out})\frac{\Delta p}{f}\right) \quad (15)$$

where $y_{ETim}(P)$ is the ordinate of the principal point relative to $(E_i, \mathbf{i}_{ETim}, \mathbf{j}_{ETim})$, Δp is the size of the pixels and f is the focal length of the lens. The expression of this angular bias was demonstrated in Villette (2006).

Combining Eqs. (12) and (15) yields:

$$\theta_{out} = \arctan\left(\frac{\sin\theta_{out\_im}}{\cos\theta_{out\_im} + y_{ETim}(P)(\Delta p/f)(\tan\Omega/\cos\alpha_{lv})}\right) \quad (16)$$

This relationship demonstrates that the horizontal outlet angle can be deduced without any bias from the apparent outlet angle measured in the image when the intrinsic camera parameters and the disc configuration are known.

3. Materials and methods

3.1. *Experimental arrangement and motion-blurred images*

To measure horizontal outlet angles, a simple imaging system was developed to capture an image of the trajectories followed by the fertiliser particles in the vicinity of a spinning disc. The device was not developed using a commercial spreader, but using a custom-made experimental arrangement. The mechanical parts were made up of elements similar to those found in a common centrifugal spreader. The disc axle was set vertically. The disc was driven by an asynchronous AC motor and a programmable power supply to set the rotational speed, which was measured by a sensor. Fertiliser granules were stored in a hopper at the bottom of which a shutter sets the fertiliser flow. Under the shutter, a delivery chute adjusts the feeding point of the granules onto the disc.

The second part of the experimental arrangement consists of the imaging system which is made up of a single camera placed vertically approximately 1 m above the granule output flow (Fig. 5). This means that the camera axis is set parallel to the spinning disc axle. The camera was a monochrome digital camera Kodak Megaplus ES 1.0/MV (1008×1018 pixels). Traditional spotlights were used to illuminate the granules lengthways during their motion. The camera exposure is set long enough so that fertiliser particles appear as streaks across the image (Fig. 6). When the rotational speed of the disc was 800 rpm the exposure time was set at 35 ms. The camera was equipped with an 8.5-mm-focal-length lens which provided a field of view of approximately $1\,m \times 1\,m$ to capture a wide angular range of spreading. The lens aperture was set from f4 to f11 depending on the ambient lighting conditions. The motion-blurred images obtained with this method showed the trajectories followed by the particles in the vicinity of the disc at the beginning of their ballistic flight.

3.2. *Image processing*

As the aim of the imaging system was to extract metric information, and as image acquisition is not a perfect perspective transformation between object space and image space, each image was first corrected by using pinhole camera and lens distortion models (Heikkilä & Silvén, 1997). A previous calibration stage provided the required intrinsic camera parameters: focal length, principal point and distortion coefficients. In this way, the undistorted image can be considered as the result of a perfect pinhole model acquisition.

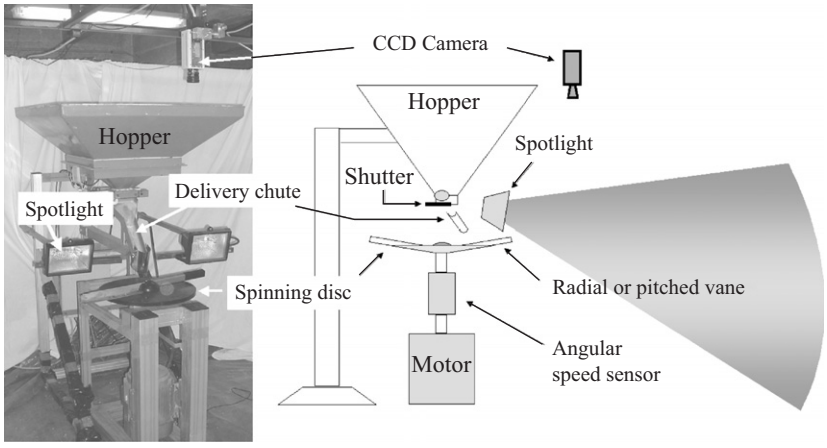

Fig. 5 – Mechanical and imaging arrangement.

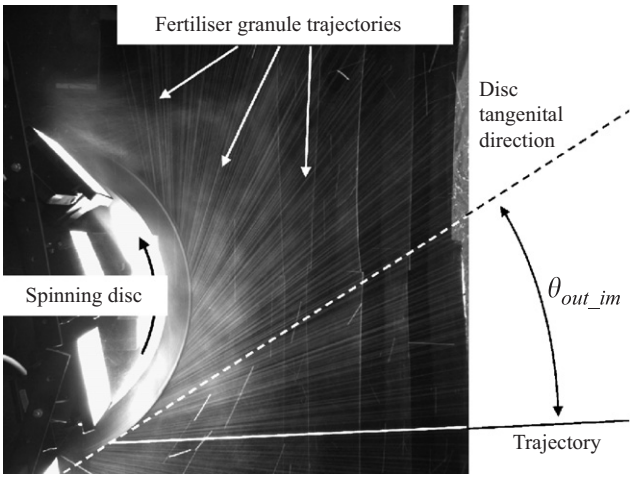

Fig. 6 – Example of motion-blurred image: θ_{out_im}, apparent outlet angle

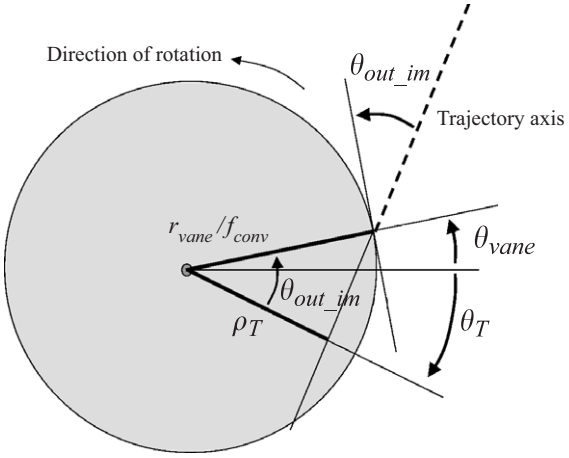

Fig. 7 – Geometrical relationship in motion-blurred images: θ_{out_im}, apparent horizontal outlet angle, θ_{vane}, angular location of the vane; θ_T angle parameter of the trajectory line; ρ_T, radius parameter of the trajectory line; r_{vane}, radius of the vane; f_{conv}, metre per pixel conversion factor.

For each image acquisition configuration, the metre per pixel conversion factor f_{conv} was determined. Moreover, the location on the CCD of the projection point A_i of the intersection point A between the disc axle and the ejection plane (i.e. the horizontal plane defined by the ejection point at the extremity of the vane) was computed. The location of this point in the image was of particular interest because the apparent outlet angle θ_{out_im} measured in the image for a specific trajectory was deduced from the distance ρ_T between this point and the trajectory axis in the image. As a matter of fact, characterising each trajectory identified in an image using the angle-radius description of a line (θ_T, ρ_T) with respect to A_i (Fig. 7), the apparent outlet angle θ_{out_im} and the angular location of the vane θ_{vane} are simply obtained as follows, whatever the vane location:

$$\theta_{out\_im} = \arccos\left(\frac{\rho_T f_{conv}}{r_{vane}}\right) \quad (17)$$

$$\theta_{vane} = \theta_T + \theta_{out\_im} \quad (18)$$

A specific image processing algorithm was developed to automatically identify a large number of trajectories and to compute the outlet angle for each of these trajectories lying in an undistorted image. The method, based on an optimised Hough transform, is described in Villette *et al.* (2006) for the case of a flat disc. Applying this method to the case of a concave disc provides only apparent outlet angles θ_{out_im} which are not horizontal outlet angles since trajectories are not parallel to the image plane. Hence, in the case of a concave disc, Eq. (16) must be used to compute the unbiased horizontal outlet angle, using the values θ_{out_im} and $y_{ETim}(P)$, which are also automatically computed for each identified trajectory in the image.

4. Results and discussion

4.1. *Preliminary static tests*

The imaging system was first assessed by means of static experiments simulating a trajectory with a physical line (i.e. tightened string) with a constant horizontal outlet angle θ_{out_sim}, for two vertical angles and various angular locations of the simulated vane. Fig. 8 illustrates the results obtained for the horizontal angle measurement when the simulated vertical angle Ω_{out_sim} was 12.4°. This shows that the bias between the simulated horizontal outlet angle and the apparent outlet angle directly measured in the image depends on the angular location of the vane. This means that it depends on the location of the simulated trajectory in the image and more precisely on the distance between the trajectory and the camera view axis. This was predicted by the theoretical approach. Fig. 8 also shows that the corrected horizontal outlet angle θ_{out}, computed using Eq. (15) and by

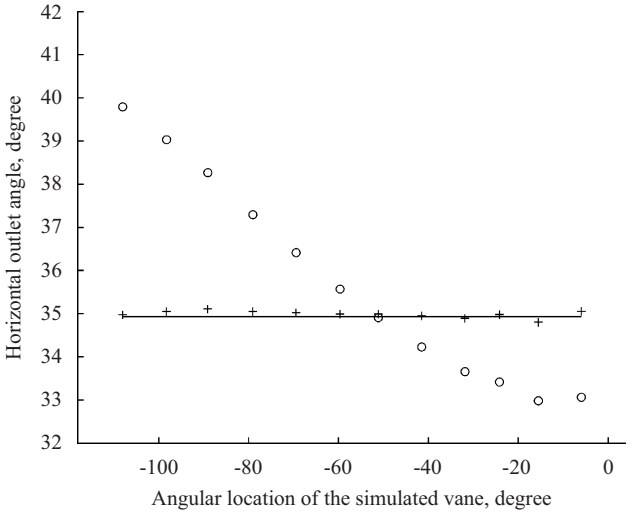

Fig. 8 – Horizontal angle of a simulated trajectory measured by computer vision: -, reference value of the horizontal angle; ○, apparent horizontal angle directly deduced from the images; +, corrected horizontal angle.

considering Ω_{out} as known, is close to the reference value, whatever the location of the vane.

The maximum differences obtained between the reference horizontal outlet angle and the values deduced from the imaging system are 0.22° and 0.18°, respectively, in two tests carried out when Ω_{out_sim} is 4.8° and Ω_{out_sim} is 12.4°. These experiments attest to a very satisfying accuracy for the computer vision method given the small impact that such an error would have for deducing outlet velocities from measured horizontal outlet angles.

4.2. *Tests with spinning discs*

The previous tests validate the image acquisition method and the use of Eq. (15) to obtain an unbiased horizontal angle measurement. Nevertheless, static experiments cannot assess the capability of the method to estimate the outlet velocity magnitude or the vertical direction of particles ejected by a spinning disc. Dynamic experiments were therefore conducted using the spreading arrangement described in Section 3.1.

It is worth noting that reference methods are not available to measure the vertical outlet angle or the three velocity components of individual millimetre-sized granules when they leave a spinning conical disc. Stroboscopic approaches using only one camera are especially ill-suited because the motion of the particles is not parallel to the image plane and the millimetre per pixel conversion factor is not constant along the trajectory image on the CCD. General laboratory methods such as particle image velocimetry (PIV) using pulsed sheets of laser light (Stanislas & Monnier, 1997) cannot easily meet our objectives since fertiliser granules are several millimetres in diameter, move in three dimensions through a wide spread area and are discontinuously ejected by the disc vanes. Consequently, two independent experiments were performed. One was performed to validate the use of the outlet angle to estimate the outlet velocity in the case of a flat disc and the other to validate the estimation of the vertical outlet angle using the horizontal outlet angle in the case of a concave disc.

4.2.1. *Outlet velocity*

In the case of a flat disc, the velocity values deduced from motion-blurred images were compared with the values obtained using a stroboscopic arrangement. For this comparison, combined images including motion streaks and stroboscopic location were acquired. To improve the accuracy concerning the location of the stroboscopic position of the particles in the image and to assure the same drag coefficient as well as a similar velocity for each particle, the test was performed with calibrated spheres (i.e. 6 mm diameter). The spinning disc was equipped with V-profile vanes ($r_{vane} = 400$ mm, $r_p = -24$ mm, $\Omega = 0°$) and the rotational speed was 800 rpm. For the approximately sixty trajectories that were studied, the mean velocity and the standard deviation obtained by the two methods were substantially the same. The velocity was 43.7 m s^{-1} and the standard deviation was 0.6 m s^{-1}. Nevertheless, when comparing the velocity estimations for each trajectory, the standard deviation of the estimated differences was 0.58 m s^{-1}, that is to say approximately 1.3% of the global mean velocity. This means that considering only a single trajectory, the two methods do not provide exactly the same velocity estimation. However, when considering a group of trajectories, the mean velocity estimated by both methods is the same. In the case of a flat disc, for both methods, the vertical outlet angle is assumed to be zero, but in practice this hypothesis is not verified for each trajectory (despite the use of a flat disc and V-profile vanes). This could explain some of the differences found in the velocity estimations between the two approaches when individual values are compared for each trajectory.

4.2.2. *Vertical outlet angle*

In the case of a concave disc, the mean value of the vertical outlet angle deduced from motion blurred images was compared with the vertical outlet angle deduced from the height of fertiliser impacts on a screen placed in the vicinity of the disc. The spreading system featured a concave disc equipped with forward-pitched V-profile vanes ($r_{vane} =$ 391 mm, $r_p = -24$ mm; $\Omega = 10.7°$). The tests were carried out using potassium chloride for various disc rotational speeds: 500, 600, 700 and 800 rpm. For each rotational speed, several images were acquired to provide approximately 200 identified and analysed trajectories. For each of these trajectories, the unbiased horizontal outlet angle was computed. Then, the outlet velocity magnitude and the vertical outlet angle were deduced. Concerning the fertiliser impact measurement on the screen, the locations of the impacts were captured using a sheet of paper covered by a carbon film. The vertical location of the paper was measured with respect to the vane so that the height of the impacts was known relative to the outlet altitude of the fertiliser. An algorithm was developed to measure the mean value of the height of the impact traces on the recording paper after scanning.

In order to compare the mean value of the vertical outlet angle deduced from images with the vertical angle corresponding to the mean height of impacts on the recording paper, the theoretical ballistic flight of the mean particle was computed. The length of the flight between the vane extremity and the corresponding impact was deduced from the distance between the disc axle and the screen, the radius of the vane and the horizontal outlet angle which is provided by the imaging system. Regarding the ballistic flight, the equation of motion is

$$\boldsymbol{a}_b = \boldsymbol{g} - K_a v_b^2 \frac{\mathbf{v}_b}{\|\mathbf{v}_b\|} \tag{19}$$

where

$$K_a = \frac{1}{2m} C_D A_p \rho_{air} \tag{20}$$

$\boldsymbol{a}_b$ and $\boldsymbol{v}_b$ are, respectively, the acceleration and the velocity vectors of the particle during the ballistic flight, m is the particle mass, C_D is the drag coefficient, A_p is the particle frontal area and ρ_{air} is the air density.

Considering a spherical particle of diameter d and density ρ_{part}, Eq. (20) yields:

$$K_a = \frac{3}{4} C_D \frac{\rho_{air}}{\rho_{part}} \frac{1}{d} \tag{21}$$

Because of their shapes, fertiliser granules cannot be considered as pure spherical particles. Thus, Eq. (21) is

modified by considering C_D as the drag coefficient of a sphere and replacing d by d_e the diameter of the equivalent sphere (i.e. the diameter of a sphere having the same aerodynamic properties as the fertiliser granules). Defining the corresponding diameter d_c of the fertiliser particle as the diameter of the sphere having the same mass and the same density, the ratio $q = d_e/d_c$ was estimated using fall tests by Grift *et al.* (1997) for various fertilisers. Considering that this q-factor is approximately 0.62 (Grift *et al.*, 1997) for potassium chloride, K_a was estimated at $0.09\,m^{-1}$ for the mean size particle of the fertiliser. It was verified that the value chosen for K_a has little influence on the height of the computed trajectory in the vicinity of the disc relative to the influence of the vertical outlet angle. For example, considering $\Omega_{out} = 5^\circ$, $v = 30\,m\,s^{-1}$ and a flight length of 1 m, the height variation obtained by increasing K_a by 100% is less than the variation obtained by decreasing Ω_{out} by 0.05°.

Table 1 provides the mean values of the vertical outlet angle Ω_{out} and the outlet velocity magnitude v deduced from the horizontal outlet angle measurements using computer vision. It also provides the vertical outlet angle values deduced from impact-recording papers when the screen is placed at 1.102 m from the disc axle. In order to appreciate the effect of the differences between the angle measured using the imaging system and the angle deduced from the screen, the corresponding theoretical variations in terms of flight length ΔL_f are computed when the ejection height is 700 mm. Table 1 shows that the greatest difference regarding the vertical outlet angle estimations is 0.17° and the greatest theoretical difference concerning the length of the ballistic flight would be 0.11 m. These findings prove that the mean value of the vertical outlet angle is derived from the horizontal outlet angle with satisfying accuracy. It can be noted that in these experiments, the vertical outlet angle is approximately half of the vertical angle of the vane. This underlines the fact that the vertical angle of fertiliser particles when they leave the vane differs significantly from the vertical angle of the vane ($\Omega = 10.7^\circ$).

Regarding the standard deviation of the vertical angle, the values obtained by computer vision are under-estimated relative to those deduced from impact recording. This means that some random variations exist around the mean value provided by the theoretical relationship (Eq. (16)). In practice, the real vertical outlet angle may be affected by several secondary parameters such as interactions between the particle shape and the extremity of the vane, vibrations of the vane or air turbulence. Also, all fertiliser particles do not leave the vane at exactly the same place on the vane extremity even when V-profile vanes are used. This contributed to an increase in height variations on the impact screen.

4.3. *Three-dimensional velocity components*

In the case of a concave disc fed with potassium chloride, the three components of the outlet velocity were deduced from the horizontal outlet angle using motion-blurred images. The rotational speed was 800 rpm and the concave disc was equipped with radial vanes with U-profiles ($r_{vane} = 287$ mm, $r_p = 0$ mm; $\Omega = 10.7^\circ$). Fig. 9 shows the three components and the total value of the velocity deduced from 32 motion-blurred images providing approximately 2500 characterised trajectories. It should be noticed that plotting velocity against the angular position of the vane during spreading did not reveal any significant increase or decrease. As a matter of fact, no significant trend was observed between the mean value of the horizontal outlet angle and the angular location of the vane during spreading. This finding differs from the results obtained by Reumers *et al.* (2003a), who used several photographic fields of view to cover the angular range of spreading and directly measured the angle on photographic images of the particle flow.

Fig. 9 also shows that the dispersion of the velocity values appears higher at the beginning and at the end of the spreading sector. This may be explained by the more individual particle motions, which are more dispersed on the vane, occurring during these phases. At the start of the spreading sector, some dispersion also occurs because some particles are incorrectly taken up by the vane.

5. Conclusions

To determine the three-dimensional components of the velocity of fertiliser particles when they leave the vane of a spinning disc, a method based on kinematic analysis has

Table 1 – Comparison of the vertical outlet angle values deduced from the horizontal outlet angle measured by computer vision and values deduced from the interception screen

$\dot{\theta}$ (rpm)	Computer vision				Interception screen			
	Ω_{out} (deg.)	$\sigma\Omega_{out}$ (deg.)	v ($m\,s^{-1}$)	L_f (m)	Ω_{out} (deg.)	$\sigma\Omega_{out}$ (deg.)	$\Delta\Omega_{out}$ (deg.)	ΔL_f (m)
500	4.91	0.19	23.7	9.5	4.76	0.67	0.15	0.07
600	4.99	0.17	28.6	11.2	4.92	0.70	0.07	0.04
700	5.07	0.19	33.5	12.8	5.11	0.69	−0.04	−0.03
800	5.04	0.17	38.2	14.2	5.21	0.67	−0.17	−0.11

$\dot{\theta}$, rotational speed of the disc; Ω_{out} vertical outlet angle; $\sigma\Omega_{out}$, standard deviation of the vertical outlet angle; v outlet velocity; L_f, theoretical length of the ballistic flight; $\Delta\Omega_{out}$, difference between the vertical angle obtained by the two methods; ΔL_f, theoretical difference concerning the flight length predicted by the two methods.

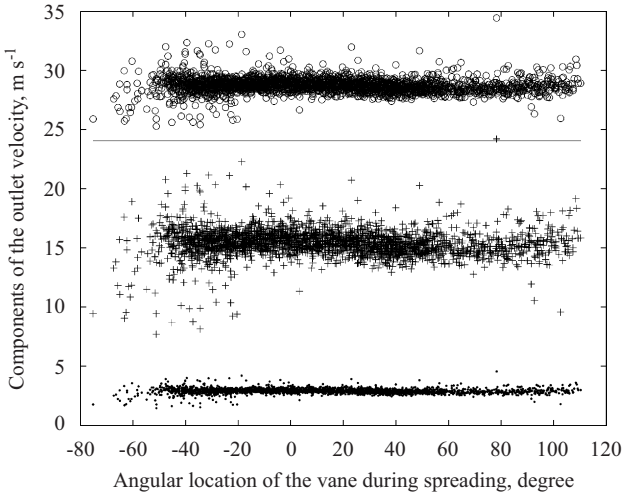

Fig. 9 – Total outlet velocity and its components with respect to the angular location of the vane during spreading: ○, total velocity; -, tangential velocity; +, radial velocity; ●, vertical velocity.

been developed. This analysis demonstrates that every velocity component can be deduced from the horizontal outlet angle measurement, the rotational speed value and the dimensional features of the vane. The study also led to the establishment of a simple theoretical relationship between the vertical and the horizontal outlet angles.

As the horizontal outlet angles of the fertiliser particles derive from their dynamic behaviour on the vane and as these angles are measured, the method does not require any assumption concerning the friction coefficient of the particles on the vane.

A computer vision method was refined to deduce the horizontal outlet angle from motion-blurred images capturing a wide angular range of spreading. Corrections were taken into account to avoid angular bias inherent in the image acquisition geometry and the lack of parallelism between the particle trajectories and the image plane in the case of a concave disc.

Experiments were carried out to show that the measurement technique provides satisfying accuracy in terms of the theoretical error concerning the prediction of the ballistic length with respect to the error concerning the estimated parameters.

In future research, ballistic flight lengths derived from three-dimensional velocity measurements and aerodynamic parameter values will be compared to real spread patterns to assess not only the measurement method but also ballistic flight computing. Furthermore, in conjunction with an angular distribution estimation method, this method of measurement is expected to lead to the development of spreader test tools for analysing spreading quality and the development of sensors for feedback loop adjustments.

Acknowledgements

The authors wish to thank Richard Martin for his work concerning the test facility and for his help in carrying out the experiments. They also thank Philippe Zwaenepoel from Cemagref and Michel Paindavoine from the University of Burgundy for their valuable comments during various stages of this work.

Appendix A. Model coefficient expressions

The general expressions of the dynamic model established by Villette *et al.* (2005) are:

$$K = \frac{\mu g \cos\Omega + g\sin\Omega - \mu r_p \dot{\theta}^2}{\dot{\theta}^2 \cos\Omega(\cos\Omega - \mu\sin\Omega)},$$
$$\delta = \sqrt{\cos^2\Omega(\mu^2+1) - \mu\sin\Omega\cos\Omega} \quad \text{(A1)}$$

Appendix B. Limiting values of the horizontal outlet angle

Considering the friction coefficient μ included between 0 and 1 and substituting these values into Eqs. (13) and (A1), the minimum and maximum values of the horizontal outlet angle are:

$$\theta_{out\_min} = \arctan\left(\frac{(l_{vane} - K_1)(\delta_1 - \cos\Omega) l_{vane}\cos^2\Omega}{r_{vane}^2 - (l_{vane} - K_1)(\delta_1 - \cos\Omega) r_p \cos\Omega}\right)$$

$$\theta_{out\_max} = \arctan\left(\frac{\delta_2(l_{vane} - K_2) l_{vane}\cos^2\Omega}{r_{vane}^2 - \delta_2(l_{vane} - K_2) r_p \cos\Omega}\right)$$

where K_1, δ_1, K_2 and δ_2 are coefficients whose expressions are as follows:

$$K_1 = \frac{g(\cos\Omega + \sin\Omega) - r_p\dot{\theta}^2}{\dot{\theta}^2\cos\Omega(\cos\Omega - \sin\Omega)}$$

$$\delta_1 = \sqrt{2\cos^2\Omega - \sin\Omega\cos\Omega}$$

$$K_2 = \frac{g\sin\Omega}{\dot{\theta}^2\cos^2\Omega}$$

$$\delta_2 = \cos\Omega$$

REFERENCES

Cointault F; Vangeyte J (2005). Photographic imaging systems to measure fertiliser granule velocity during spreading. The International Fertiliser Society, proceeding 555

Colin A (1997). Etude du procédé d'épandage centrifuge d'engrais minéraux. [Study of mineral fertiliser centrifugal spreading.] PhD Thesis, Université de Technologie de Compiègne, France

Cunningham F M (1963). Performance characteristics of bulk spreaders for granular fertilizer. Transactions of the ASAE, **6**(2), 108–114

Cunningham F M; Chao E Y S (1967). Design relationships for centrifugal fertilizer distributors. Transactions of the American Society of Agricultural Engineers, **10**(1), 91–95

Dintwa E; Van Liedekerke P; Olieslagers R; Tijskens E; Ramon H (2004). Model for simulation of particle flow on a centrifugal fertiliser spreader. Biosystems Engineering, **87**(4), 407–415, doi:10.1016/j.biosystemseng.2003.12.009

Grift T E; Hofstee J W (1997). Measurement of velocity and diameter of individual fertilizer particles by an optical

method. Journal of Agricultural Engineering Research, **66**(3), 235–238, doi:10.1006/jaer.1996.0128

Grift T E; Hofstee J W (2002). Testing an online spread pattern determination sensor on a broadcast fertiliser spreader. Transactions of the American Society of Agricultural Engineers, **45**(3), 561–567

Grift T E; Kweon G; Hofstee J W; Piron E; Villette S (2006). Dynamic friction coefficient measurement of granular fertiliser particles. Biosystems Engineering, **95**(4), 507–515, doi:10.1016/j.biosystemseng.2006.08.006

Grift T E; Walker J T; Hofstee J W (1997). Aerodynamic properties of individual fertilizer particles. Transactions of the American Society of Agricultural Engineers, **40**(1), 13–20

Heikkilä J; Silvén O (1997). A four-step camera calibration procedure with implicit image correction. IEEE Computer Society Conference on Computer Vision and Pattern Recognition (CVPR'97), pp 1106–1112. San Juan, Puerto Rico.

Hofstee J W (1992). Handling and spreading of fertilizers: part 2, physical properties of fertilizer, measuring methods and data. Journal of Agricultural Engineering Research, **53,** 141–162, doi:10.1016/0021-8634(92)80079-8

Hofstee J W (1994). Handling and spreading of fertilizers: part 3, measurement of particle velocities and directions with ultrasonic transducers, theory, measurement system, and experimental arrangements. Journal of Agricultural Engineering Research, **58**(1), 1–16, doi:10.1006/jaer.1994.1030

Hofstee J W (1995). Handling and spreading of fertilizers: part 5, the spinning disc type fertilizer spreader. Journal of Agricultural Engineering Research, **62**(3), 143–162, doi:10.1006/jaer.1995.1073

Hofstee J W; Huisman W (1990). Handling and spreading of fertilizers: part 1, physical properties of fertilizer in relation to particle motion. Journal of Agricultural Engineering Research, **47**(4), 213–234, doi:10.1016/0021-8634(90)80043-T

Inns F M; Reece A R (1962). The theory of centrifugal distributor, II: motion on the disc, off-centre feed. Journal of Agricultural Engineering Research, **7**(4), 345–353

Leterme P -Y (2000). Précision des épandages: une situation contrastée. [Spreading accuracy: a contrasted situation.]. Perspectives Agricoles, **263,** 62–64

Olieslagers R (1997). Fertilizer distribution modelling for centrifugal spreader design. PhD Thesis, nr. 341, aan de faculteit der landbouwwetenschappen, K.U. Leuven, Belgium

Olieslagers R; Ramon H; De Baerdemaeker J (1996). Calculation of fertilizer distribution patterns from a spinning disc spreader by means of a simulation model. Journal of Agricultural Engineering Research, **63**(2), 137–152, doi:10.1006/jaer.1996.0016

Patterson D E; Reece A R (1962). The theory of the centrifugal distributor, I: Motion on the disc, near-centre feed. Journal of Agricultural Engineering Research, **7**(3), 232–240

Reumers J; Tijskens E; Ramon H (2003a). Experimental characterisation of the tangential and cylindrical fertiliser distribution pattern from a spinning disc: a parameter study. Biosystems Engineering, **86**(3), 327–337, doi:10.1016/j.biosystemseng.2003.08.004

Reumers J; Tijskens E; Ramon H (2003b). Experimental characterisation of the cylindrical distribution pattern of centrifugal fertiliser spreaders: towards an alternative for spreading hall measurements. Biosystems Engineering, **86**(4), 431–439, doi:10.1016/j.biosystemseng.2003.09.002

Roussel D (2006). Spreader field tests: the Dynatest method and spreading practices observations. Proceedings of the 2nd International Symposium on centrifugal fertiliser spreading. October 24–25, 2006, Montoldre, France

Stanislas M; Monnier J -C (1997). Practical aspects of image recording in particle image velocimetry. Measurement Science and Technology, **8,** 1417–1426

Tijskens E; Van Liederkerke P; Ramon H (2005). Modelling to aid assessment of fertiliser handling and spreading characteristics. The International Fertiliser Society, proceeding 553

Tissot S; Miserque O; Mostade O; Huyghebaert B; Destain J P (2002). Uniformity of N-fertiliser spreading and risk of ground water contamination. Irrigation and Drainage, **51,** 17–27

Tissot S; Queron G; Miserque O (1999). Tolérance d'une culture de froment à l'égard de l'hétérogénéité d'épandage des engrais azotés. [Tolerance of wheat crop towards the spreading heterogeneity of nitrogen manure.]. Biotechnology Agronomy Society Environment, **3**(3), 247–252

Van Liedekerke P; Tijskens E; Ramon H (2005). DEM modeling of centrifugal fertilizer spreading. Proceedings of the 1st International Symposium on Centrifugal Fertiliser Spreading, September 15–16, 2005, Leuven, Belgium

Villette S; Cointault F; Chopinet B; Paindavoine M (2006). Optimizing Hough transform for fertilizer spreading optical control. Optical Engineering, **45**(2), Article no. 027006

Villette S; Cointault F; Piron E; Chopinet B (2005). Centrifugal spreading: an analytical model for the motion of fertiliser particles on a spinning disc. Biosystems Engineering, **92**(2), 157–164, doi:10.1016/j.biosystemseng.2005.06.013

Villette S (2006). Estimation de vitesse par analyse d'images acquises en filé: application à la caractérisation de la distribution centrifuge de granules d'engrais. [Velocity estimation using motion blurred images: Application to the characterisation of centrifugal distribution of granular fertiliser.] PhD Thesis, Université de Bourgogne, France

Ziani S; Rousselet M (1990a). Epandage des engrais et verse des céréales. [Fertiliser spreading and cereal lodging.]. Bulletin Technique du Machinisme et de l'Equipement Agricoles, **45,** 28–38

Ziani S; Rousselet M (1990b). Qualité de l'épandage d'engrais—Enquête auprès des agriculteurs du Val d'Allier. [Quality of fertiliser spreading—Investigation with farmers from Val d'Allier.]. Bulletin Technique du Machinisme et de l'Equipement Agricoles, **48,** 9–17